PIF7-mediated epigenetic reprogramming promotes the transcriptional response to shade in Arabidopsis

Chuanwei Yang, Tongdan Zhu, Nana Zhou, Sha Huang, Yue Zeng, Wen Jiang, Yu Xie, Wen-Hui Shen, Lin Li

PHYTOCHROME-INTERACTING FACTOR 7-mediated epigenetic reprogramming promotes the transcriptional response to shade in *Arabidopsis*

Chuanwei Yang[1], Tongdan Zhu[1], Nana Zhou[2], Sha Huang[1], Yue Zeng[1], Wen Jiang[2], Yu Xie[1], Wen-Hui Shen[3], and Lin Li[1,*]

[1]State Key Laboratory of Genetic Engineering, Institute of Plants Biology, School of Life Sciences, Fudan University, Shanghai 200438, People's Republic of China

[2] State Key Laboratory of Genetic Engineering, Department of Biochemistry, Institute of Plants Biology, School of Life Sciences, Fudan University, Shanghai 200438, People's Republic of China

[3]Institut de Biologie Moléculaire des Plantes, CNRS, Université de Strasbourg, Strasbourg 67084, France

[*]Corresponding Authors: linli@fudan.edu.cn

Abstract

For shade-intolerant plants, changes in light quality are taken as indicative of competitions from neighbors and thus trigger shade avoidance syndrome (SAS), with a series of morphological and physiological alterations that are detrimental to plant health and consequently crop yield. PYHTOCHROME-INTERACTING FACTOR 7 (PIF7) is a major transcriptional regulator of SAS in *Arabidopsis*. Here, we show that PIF7 directly interacts with the histone chaperone ANTI-SILENCING FACTOR 1 (ASF1). The ASF1-deprived *asf1ab* mutant showed defective shade-induced hypocotyl elongation. HISTONE REGULATOR HOMOLOG A (HIRA), which mediates deposition of the H3.3 variant into chromatin, is also involved in SAS. RNA/ChIP-sequencing analyses identified ASF1 directly regulating a subset of target genes of PIF7. Furthermore, shade-elicited gene activation is accompanied by H3.3 enrichment, which is mediated by the PIF7-ASF1-HIRA regulatory module. Collectively, our data reveal that PIF7 recruits ASF1-HIRA to increase H3.3 incorporation into chromatin to promote gene transcription, thus enabling plants to effectively respond to environmental shade.

Key words: ASF1 / H3.3 incorporation / HIRA / PIF7 / shade avoidance

Introduction

Plants are sessile organisms that adapt to various strategies by altering their growth and development in response to environmental changes. As photosynthetic organisms, plants are particularly sensitive to local light environments. Light influences every developmental transition, from seed germination and seedling emergence to flowering, reproduction, and seed formation. Shade-intolerant plants can detect the proximity and density of neighboring vegetation through perception of a reduced ratio of red (660 nm) to far red (730 nm) light, which triggers the shade avoidance syndrome (SAS) that includes responses, such as an increase in hypocotyl and internode elongation, extended petioles, and changes in leaf hyponasty (Casal, 2013; Ruberti et al., 2012). Prolonged shade exposure can lead to early flowering, reduced branching, and decreased seed yields (Fernandez-Milmanda and Ballare, 2021; Galvao et al., 2019; Zhang et al., 2019). As an adaptive strategy, SAS allows shaded plants to grow and compete with their neighbors at the cost of grain yield or plant biomass.

In *Arabidopsis thaliana*, shade-light filtered through dense planting is perceived by photoreceptors (mainly known as phytochromes). The constitutive SAS phenotype of *phytochrome B (phyB)* mutant indicates that phyB plays a dominant role in inhibiting SAS (Reed et al., 1993). Shade-light drives the Pfr-to-Pr conversion of phyB, allowing dephosphorylation and accumulation of PHYTOCHROME-INTERACTING FACTORS (PIFs), a family of basic helix-loop-helix (bHLH) transcription factors (Leivar and Quail, 2011; Paik et al., 2017). The activation of PIFs, especially PIF7, promotes shade-induced gene expression and SAS (Galvao et al., 2019; Li et al., 2012; Zhang et al., 2019). Numerous studies have been reported about the transcriptional activity and function (Jiang et al., 2019; Li et al., 2012; Peng et al., 2018; Willige et al., 2021; Yang et al., 2021), translation (Chung et al., 2020), subcellular localization (Huang et al., 2018), and protein stability (Zhou

et al., 2021) of PIF7, which have helped on understanding the molecular mechanisms of SAS.

Yeast two-hybrid (Y2H) assays, conducted in our previous study (Huang et al., 2018), revealed that ANTI-SILENCING FUNCTION 1 (ASF1) is one of the putative PIF7-interacting proteins. ASF1 is an evolutionarily conserved histone chaperone of the H3/H4 family (English et al., 2006; Natsume et al., 2007). The molecular functions and biochemical mechanisms of ASF1 have been well studied in animals and yeast. At DNA replication forks, ASF1 plays an important role in regulating the supply of H3.1 and H4 to the CHROMATIN ASSEMBLY FACTOR 1 (CAF1) in chromatin assembly (Eitoku et al., 2008; English et al., 2006; Otero et al., 2014). ASF1 also provides H3.3-H4 dimers to HISTONE REGULATORY HOMOLOG A (HIRA) for DNA replication-independent nucleosome assembly. While the canonical H3.1 is incorporated during DNA replication, the histone variant H3.3 is mainly incorporated upon gene activation and enriched in chromatin at actively transcribed genes (Ahmad and Henikoff, 2002; McKittrick et al., 2004; Shu et al., 2014; Stroud et al., 2012). Yeast cells lacking *ASF1* display increased frequency of genome instability (Prado et al., 2004; Ramey et al., 2004). Deficiency of *ASF1* in vertebrates and flies leads to embryonic lethality (Moshkin et al., 2002; Schulz and Tyler, 2006).

Two ASF1-homologs (ASF1A and ASF1B) are found in *Arabidopsis*, which play redundant roles and are shown to participate in S-phase DNA replication-dependent chromatin assembly (Zhu et al., 2011). The loss-of-function *asf1ab* double mutant exhibits defective thermo tolerance (Weng et al., 2014) and early-flowering phenotypes (Zhao et al., 2021). Many HIRA-regulated genes were found belonging to a broad class of responsive genes to the environmental changes (Duc et al., 2017; Nie et al., 2014), however, whether and how ASF1 and HIRA coordinately regulate the transcription of specific genes in plants is still poorly understood.

In this study, we report that ASF1 and HIRA are required for shade-induced hypocotyl elongation. Our results indicated that ASF1 is recruited by PIF7 to bind to a cluster of shade-responsive genes. The PIF7-ASF1-HIRA complex promotes transcription by depositing H3.3 into chromatin at the target genes. Combined with previous reports (Peng et al., 2018; Willige et al., 2021), our study brings out that PIF7 recruits different chromatin modulators and conducts diverse types of histone variants (H3.3 and H2A.Z) and modifications to reprogram chromatin structure in response to shade.

Results

PIF7 interacts with ASF1A and ASF1B

Before verifying the interaction between PIF7 and ASF1, we first determined the effect of light on *ASF1* expression. In *Arabidopsis*, ASF1A and ASF1B showed high sequence conservation (approximately 77.44% similarity) (Appendix Fig S1A). Both *ASF1A* and *ASF1B* mRNA levels were found stable in Col-0 and *pif7* under different light/shade/dark treatments (Appendix Fig S1B), which is consistent with the published RNA sequencing (RNA-seq) data (Appendix Fig S1C, GSE81202). To investigate the effects of light on ASF1A and ASF1B protein abundance, 6-d-old white light-grown *35S::GFP-ASF1A* and *35S::ASF1B-GFP* transgenic seedlings were transferred from white light to shade for 2 h. The protein levels of ASF1A and ASF1B (Appendix Fig S1D-E) were found barely changed after shade treatment. Together, these observations indicate that light does not significantly affect the transcription and protein levels of ASF1.

To test the interaction between PIF7 and ASF1, we used a luciferase complementation imaging (LCI) assay. As shown in Fig 1A, cLUC-tagged PIF7 could interact with nLUC-tagged ASF1A or ASF1B when they were transiently expressed in *Nicotiana benthamiana* leaf cells. In an *in vitro* pull-down assay,

SUMO-His-PIF7 was bound by GST-fused ASF1A or ASF1B (Fig 1B, Appendix Fig S2A). In a semi-*in vivo* pull-down assay, GFP-ASF1A extracted from *GFP-ASF1A* seedlings were found to be bound by TF-His-PIF7 proteins purified from *E. coli* (Appendix Fig S2B). Interestingly, the dephosphorylated, but not the phosphorylated, PIF7-Flash (9×Myc-6×His-3×Flag) extracted from *35S:PIF7-Flash* (Li et al., 2012) seedlings, was found to be bound by the GST-fused ASF1 (Fig 1C). Finally, to further examine the interaction between ASF1 and PIF7 *in vivo*, we crossed the *GFP-ASF1A* line with *PIF7-Flash* line and performed the co-immunoprecipitation (Co-IP) assays. As expected, we found that GFP-ASF1A formed protein complexes with dephosphorylated PIF7-Flash (Fig 1D, Appendix Fig S2C). Taken together, these data strongly indicate that PIF7 physically interacts with ASF1, both *in vitro* and *in vivo.*

Because human ASF1 and HIRA form protein complexes (Tang et al., 2006), we also tested the interactions of *Arabidopsis* HIRA with ASF1 and PIF7. We first confirmed the interaction between *Arabidopsis* ASF1A and HIRA by performing an *in vitro* pull-down assay using TF-His-HIRA and GST-ASF1A (Fig 1E, Appendix Fig S2A). We further found that TF-His-HIRA could also be pulled down by GFP-PIF7, albeit to a lesser extent (Appendix Fig S2D). Lastly, GFP-ASF1A simultaneously precipitated both HIRA-HA and PIF7-Flash when co-expressed in tobacco leaves (Fig 1F). Based on these observations, we conclude that ASF1, HIRA and PIF7 together form a multiple-protein complex.

The histone chaperone ASF1 and HIRA positively regulate shade-induced hypocotyl elongation

To investigate the function of ASF1 in SAS, we examined the hypocotyl phenotypes of the *asf1a-2*, *asf1b-1*, and *asf1a-2asf1b-1* (*asf1ab*) mutants (Zhu et al., 2011). Although the single mutant *asf1a-2* and *asf1b-1* showed no difference in shade-induced hypocotyl elongation compared to the wild-type

Col-0, the double mutant *asf1ab* displayed a shade-defective phenotype, similar to that of *pif7-1* (Fig 2A). The *hira-1* was lesser shade-defective than *asf1ab*. The *pif7-1*, *asf1ab*, and *hira-1* seedlings all showed reduced growth and slower growth rates than Col-0 seedlings during the first 10 h after shade treatment (Fig 2B-C), indicating that these components are involved in promoting early shade response.

To determine the relationship of ASF1 and HIRA with phyB, we generated *asf1ab * phyB-9* and *hira-1 * phyB-9* mutants by crossing. These combined mutants showed shorter hypocotyls than *phyB* under white light conditions (Fig 2D), indicating that the function of the photoreceptor phyB partially relies on ASF1 and HIRA.

To investigate the functional interactions between PIF7 and ASF1, we crossed *asf1ab* and *hira-1* with *pif7-1*, respectively. As expected, the *asf1ab * pif7-1* and *hira-1 * pif7-1* mutants showed hypocotyl lengths that were similar to that of *pif7-1* (Fig 2E), suggesting that the function of ASF1 and HIRA in shade-induced hypocotyl growth depends on PIF7.

In addition to SAS, PIF7 is also important for early responses to elevated temperature in *Arabidopsis* seedlings (Burko et al., 2022; Chung et al., 2020; Fiorucci et al., 2020). We found defective hypocotyl elongation of *asf1ab* and *hira-1* at 29°C (Appendix Fig S3), suggesting that the PIF7-ASF1-HIRA complex may also play a role in thermomorphogenesis besides shade response. Nonetheless, hereinafter, we focus on shade response to uncover molecular mechanism underlying the PIF7-ASF1-HIRA regulation in hypocotyl elongation.

PIF7, ASF1, and HIRA are involved in shade-induced gene expression

To investigate the roles of ASF1 and HIRA in shade-induced transcription, we performed RNA-seq analysis in *asf1ab* and *hira-1* mutants, compared it with *pif7-1* (Appendix Fig S4A-C). After 1 h shade stimuli, 642 shade-induced

genes were identified in Col-0 seedlings (fold change > 2 and *P*-value < 0.01, Dataset EV1). The expression of these genes was compromised in *pif7-1*, as well as in *asf1ab* and *hira-1* mutants to varying degrees (Fig 3A-B, Dataset EV1). Specifically, there are 374, 222, and 258 genes showing reduced shade induction in *pif7-1*, *asf1ab*, and *hira-1*, respectively (Fig 3C, Dataset EV2). Hereinafter we called these genes as PIF7-regulated, ASF1-regulated and HIRA-regulated shade-responsive genes, respectively. Furthermore, 132 common genes showed reduced shade induction in all three mutants (Fig 3C). Gene ontology (GO) analysis revealed that these common genes were enriched in functional categories, including auxin-activated signaling pathway, response to auxin, and transcription DNA-templated (Fig 3D, Table EV1).

Remarkably, in response to shade stimuli, 77.2%, 66.7%, and 70.8% of differentially expressed genes (DEGs) were down-regulated in *pif7-1*, *asf1ab*, and *hira-1*, respectively, indicating a positive effect of PIF7, ASF1, and HIRA on the transcriptional activation of these genes under shade (Appendix Fig S4D, Dataset EV3). Among the identified DEGs, the expression patterns of light related genes (*ATHB2*, and *NPY8*), hormone related genes (*PIN7*, *BIM1*, and *ARL*), and developmental growth-related genes (*CSLC4*) were further verified and confirmed using quantitative RT-PCR analysis (Appendix Fig S4E). Based on the RNA-seq and qRT-PCR data, we conclude that PIF7, ASF1, and HIRA act in transcriptional activation and regulate a substantial common subset of shade-related genes.

Shade increases ASF1-enrichment in the chromatin of target genes of PIF7

To investigate the chromatin-binding activity of ASF1 in response to shade exposure, we performed chromatin immunoprecipitation sequencing (ChIP-seq) analysis using anti-GFP antibodies on white light- and shade-grown *GFP-ASF1A* transgenic *Arabidopsis* plants. Approximately 6,259

peaks (for 5,662 genes) under white light and 9,031 peaks (for 7,950 genes) after 1 h of shade treatment were identified as high-confidence GFP-ASF1A-enriched peaks (Fig 4A, fold change > 1.5, *P*-value < 0.01, Dataset EV4). Examination of shade-induced GFP-ASF1A-enrichment distributions revealed that 57.24% of the binding occurred at the coding exon, and 29.91% of them were found at the promoter (Fig 4B, Dataset EV5).

The numbers of GFP-ASF1A-enriched peaks were slightly increased under shade. Compared to that in white light conditions, the genome-wide GFP-ASF1A-enriment was increased in response to shade. Specifically, 2,701 peaks (for 2,566 genes) showed an increase (fold change > 1.5, *P*-value < 0.01; Dataset EV5), and these corresponding genes are called here after referred to as shade-induced GFP-ASF1-bound genes. We found 161 shade-induced GFP-ASF1-bound genes (average density plot shown in Appendix Fig S5A) that overlapped with DEGs in *asf1ab* (gene list in Dataset EV3 and EV5), thus likely representing genes that are directly regulated by ASF1 (GFP-ASF1A-targeted genes). GO analysis revealed that these genes were over-represented by the “response to light stimulus,” and “response to auxin,” were significantly enriched (Appendix Fig S5B, Table EV2).

Specifically, GFP-ASF1A enrichment was significantly increased under shade in 642 shade-induced genes, but not at control genes (not regulated by shade; Dataset EV2) (Fig 4C). Enhancement in enrichment was more remarkable for 131 GFP-ASF1A bound genes (Appendix Fig S5C). These results indicate that for a subset of shade-induced genes shade-mediated gene activation is accompanied by ASF1 enrichment. The enrichment was illustrated as integrative genomics viewer (IGV) screen shots for the selected genes *ATHB2*, *PIN7*, *CSLC4*, *BIM1*, *ARL*, and *NPY8* (Fig 4D).

To examine the possible involvement of PIF7 in shade-induced ASF1-bindings, we examined shade-induced GFP-ASF1A enrichment for the 182 PIF7-targeted (PIF7 bound and PIF7-regulated) shade-responsive genes

(Fig 4E, Dataset EV2). A shade-enhanced enrichment of GFP-ASF1A was observed for 43 of these PIF7 targeted genes (Fig 4F, Dataset EV2), indicating that their activation is associated with PIF7.

Then, we directly investigated the role of PIF7 in the binding of ASF1 to target genes. For this, we used the anti-ASF1A antibody, which has been proven to be effective in ChIP-PCR analyses (Weng et al., 2014). Shade-induced enrichment of ASF1A at the selected genes *ATHB2*, *PIN7*, *CSLC4*, *BIM1*, *ARL*, and *NPY8* was greatly reduced in *pif7-1* (Fig 4G) and slightly reduced in *pifq* (Appendix Fig S5D), indicating that the recruitment of ASF1A relies on PIFs, particularly PIF7.

Taken together, our results indicate that PIF7 recruits ASF1 for the transcriptional activation of a subset of genes in response to shade.

Shade induces H3.3 levels at a subset of shade-responsive genes

Because ASF1 plays a role in the deposition of both H3.1 and H3.3 while HIRA is considered as specific for H3.3 (Tagami et al., 2004), we speculated that PIF7-ASF1-HIRA might regulate shade-induced gene expression by affecting the balance of H3.1 and H3.3 assembly into chromatin. As a primary step, we first performed ChIP-seq to examine the effect of shade exposure on the genome-wide landscape distribution of H3.1 and H3.3. We selected HTR13 as the representative for H3.1 and HTR5 for H3.3, both of which have been described previously (Stroud et al., 2012). We generated *pHTR13::HTR13-HA* and *pHTR5::HTR5-HA* transgenic lines and performed ChIP-seq analyses using anti-HA antibodies, and obtained H3.1 and H3.3 density patterns (Fig 5, Appendix Fig S6). Based on a cutoff fold change > 1.5 and *P*-value < 0.01, it was found that HTR13 / HTR5 was enriched in up to 10,827 peaks (for 8,746 genes) / 14,623 peaks (for 12,125 genes) under white light, and 10,842 peaks (for 8,527 genes) / 12,718 peaks (for 10,781 genes) after 1 h of shade treatment (Dataset EV6 and Dataset EV7). The occupancy of HTR13 / HTR5

detected in this study showed good overlap with previously published datasets obtained in Col-0 under white light (Wollmann et al., 2012) (Appendix Fig S6A-B). Consistent with the previous studies (Stroud et al., 2012; Wollmann et al., 2012), H3.1 was distributed across the gene body and associated with transcriptionally silent regions in the genome (Appendix Fig S6C), whereas the variant H3.3 was predominantly distributed towards the Transcriptional End Site (TES) and positively correlated with the levels of gene expression (Appendix Fig S6D).

Although the peak numbers of HTR13 and HTR5 were slightly reduced under shade, it did not affect the global levels of histone H3.1 and H3.3 (Fig 5A-B, Appendix Fig S6E), which is consistent with the stable mRNA levels of H3 genes (Appendix Fig S6F) and the protein levels of HTR13-HA and HTR5-HA detected by western-blot analysis (Appendix Fig S6G). Interestingly, for the 642 shade-induced genes, however, we found that shade increased H3.3 level (Fig 5C) and no significantly changed the H3.1 level (Fig 5D), indicating that shade-elicited gene activation is accompanied by H3.3 enrichment. As control, genes not regulated by shade (Dataset EV2) did not show changes of H3.3 and H3.1 level under shade (Fig 5C-D). In parallel, we also investigated whether shade-induced H3.3 enriched genes were shade-responsive. Thus, the 1323 peaks (1246 protein-coding genes) that displayed an increase in H3.3 level in response to shade (fold change > 1.5 and *P*-value < 0.01, Dataset EV8) were found to be transcriptionally slightly induced under shade (Fig 5E, Dataset EV9). GO analysis revealed enrichment of “response to auxin,” “transcription, DNA-templated,” and “brassinosteroid mediated pathway,” related terms for the top 400 genes with gaining H3.3 incorporation and increasing expression upon shade in Col-0 (Fig 5F, Table EV3), with the profiles of *ATHB2*, *PIN7*, *CSLC4*, *BIM1*, *ARL*, and *NPY8* showing as examples (Fig 5G).

To further examine the function of H3.3 in shade responses, we obtained an H3.3 knockdown mutant (*h3.3kd*) (Wollmann et al., 2017). *h3.3kd* displayed a defective phenotype for shade-induced hypocotyl elongation (Fig 5H), which is largely similar to *asf1ab*. Moreover, the shade-induction of *ATHB2*, *PIN7*, *CSLC4*, *BIM1*, *ARL*, and *NPY8* was impaired in *h3.3kd* (Fig 5I).

Taken together, our data indicate that activation of shade-induced genes is associated with H3.3 enrichment and that H3.3 is required for proper a subset of shade-induction gene transcription and hypocotyl elongation.

Shade-induced H3.3 enriched levels rely on PIF7-ASF1-HIRA regulatory module

Next, we examined the association of PIF7 and ASF1 functions with shade-induced H3.3 incorporation. We checked the overlap between shade-induced ASF1-bound genes, PIF7-bound genes (GSE156584) (Yang et al., 2021) and H3.3 enriched genes (Appendix Fig S7A). Genome ontology analysis of these genes showed that “regulation of transcription, DNA-templated,” “regulation of cell size,” and “shade avoidance,” were significantly enriched (Appendix Fig S7B, Table EV4). We also found that the enrichments of H3.3 were amplified by shade at PIF7-regulated shade-responsive genes, ASF1-regulated shade-responsive genes, and HIRA-regulated shade-responsive genes (Appendix Fig S7C). Moreover, shade effect on H3.3 enrichment was aggravated at PIF7-targeted shade-responsive genes (Appendix Fig S7C). Consistently, the transcriptional levels of top 400 genes with gaining H3.3 incorporation and increasing expression upon shade in Col-0 were found compromised in *pif7-1, asf1ab,* and *hira-1* (Appendix Fig S7D).

To further test the role of PIF7 in facilitating shade-induced H3.3 incorporation, we profiled H3.3 occupancy in the *pif7-1* mutant using *pHTR5::HTR5-HA/pif7-1* transgenic lines under white light and shade

conditions (Fig 6A). HTR5 was enriched in up to 16,710 peaks (for 13,418 coding genes) under white light, and 16,363 peaks (for 13,158 coding genes) after 1 h of shade treatment in *pif7-1* (with cutoff fold change > 1.5 and *P*-value < 0.01, Dataset EV10). The peaks of H3.3 detected in *pif7-1* largely overlapped with that in Col-0 (Appendix Fig S7E), suggesting that PIF7 does not affect the distribution pattern of H3.3 in the genome.

The shade-induced enrichment of H3.3 in Col-0 was clearly faint in the *pif7-1* mutant (Fig 6B). Then we calculated the shade-enhanced H3.3 levels (enrichment levels of HTR5 under shade minus the enrichment levels of HTR5 under white light) in Col-0 and *pif7-1*. For 642 shade-induced genes, shade-enhanced H3.3 enrichment was strongly compromised in the *pif7-1* mutant (Fig 6C). Moreover, H3.3 enrichments at the PIF7-targeted shade-responsive genes, at the ASF1-bound and PIF7 targeted shade-responsive genes, as well as at the HIRA-regulated shade-responsive genes were compromised in *pif7-1* compared to Col-0 (Fig 6D and Appendix Fig S7F). These results suggest that shade-enhanced PIF7 activity is a prerequisite for H3.3 deposition and subsequent gene activation.

To further verify whether shade-enhanced H3.3 levels are dependent on the PIF7-ASF1-HIRA regulatory module, we assessed HTR5 occupancy at multiple selected genes in Col-0, *pif7*-1, *asf1ab*, and *hira-1* by ChIP-PCR using *pHTR5::HTR5-HA* transgenic lines. The levels of shade-induced HTR5 enrichment were reduced in these three mutants at the 3'-ends of *ATHB2*, *PIN7*, *CSLC4*, *BIM1*, *ARL*, and *NPY8* (Fig 6E).

Taken together, these results corroborate the previously established functions of ASF1-HIRA in H3.3 deposition, thus facilitating nucleosome formation (Horard et al., 2018), and indicate that PIF7 recruits ASF1-HIRA to increase H3.3 incorporation to activate transcription on a subset of shade-induced genes.

Discussion

Plant growth and development are predominantly postembryonic and occur in response to environmental cues. This developmental plasticity is thought to be an adaptation to the sessile lifestyle of plants. SAS is an excellent example of the phenotypic plasticity in the environment. Genetic and epigenetic factors are intertwined in a complex regulatory network for environmental adaptation (Xiao et al., 2017; Zhao et al., 2020). Transcription factors play an important role in environmentally triggered transcriptional reprogramming events, in addition to acting as transcriptional switches, they can also recruit chromatin modulators to increase the precision of regulation (Zhao et al., 2020).

PIFs serve as regulatory hubs that integrate environmental cues into transcriptional scenario. In this study, we found that PIF7 directly interacts with ASF1 to promote the expression of shade-responsive genes by mediating H3.3 enrichment at the target genes of PIF7. Under shade conditions, PIF7 can also recruit histone acetylases to promote H4K5ac in some shade-induced genes, e.g., *YUC8*, *YUC9*, and *PAR1* (Peng et al., 2018). However, *YUC8*, *YUC9*, and *PAR1* showed stable levels of H3.3 enrichment under shade treatment (Appendix Fig S8A). PIF7 recruits histone acetylase and EIN6 ENHANCER (EEN) to regulate H3K9ac and H2A.Z profiles at PIF7 core genes, e.g., *ATHB2* (Willige et al., 2021). The results of our study revealed that there only a few genes showed more than one epigenetic change in response to shade or low R:FR (Appendix Fig S8B), such as *ATHB2* showing enhanced H3.3 and H3K9ac but reduced H2A.Z (Appendix Fig S8C). Therefore, PIF7 may recruit different chromatin modulators (e.g. ASF1, EEN, MRG1/2, and histone acetylase) and conducts diverse types of histone variants (H3.3 and H2A.Z) and modifications (H4K5ac and H3K9ac) in an interactive or non-interactive manner, likely depending on the target gene context, to reprogram chromatin structure under shade. These epigenetic changes might occur at different speeds in response to shade, and/or in different genes

involved in different steps/pathways of regulation of cell proliferation/expansion. The complexity of epigenetic regulatory mechanisms might be advantageous for sedentary plants to precisely control gene transcription in response to dynamic environmental changes.

Most binding peaks of PIF7 occur in the promoter region (Willige et al., 2021; Yang et al., 2021), approximately 25.1% and 6.4% of PIF7 binding events occur in exons and introns, respectively (Willige et al., 2021). Our results indicated that ASF1 binding events were mainly enriched in gene bodies (Fig 4B). Shade-induced binding events of ASF1 and H3.3 enrichment mainly occur at the 3'-end of the gene bodies (Fig 4 and 5). So how does PIF7 regulate the distribution of H3.3 on the 3'-end of the gene bodies? One hypothesis is that PIF7 bound in gene bodies can directly recruit the ASF1-HIRA complex, thereby affecting the enrichment of H3.3 and regulating gene expression. Another hypothesis is that genes can be configured as looped structures (Kadauke and Blobel, 2009). Recent studies have described that active phyB forms a repressive chromatin loop with VIN3-LIKE1/VERNALIZATION 5 (VIL1/VRN5) in growth-promoting genes (Kim et al., 2021). The enriched H3.3 at the 3'-end of *FLOWERING LOCUS C* (*FLC*) can enhance active histone modifications (H3K4me3) at the 5'-end by gene loop formation (Zhao et al., 2021). The three-dimensional genome chromatin loop structure juxtapose regulatory elements to regulate transcription with high efficiency (Kadauke and Blobel, 2009). However, whether PIF7-ASF1-HIRA affects chromatin loops at shade-responsive genes remains to be investigated further.

Our results suggest that ASF1 is involved in shade-induced hypocotyl elongation mainly by activating gene expression, which is correlated with transcriptional activation of PIF7 (Appendix Fig S4D). In this study, we found that ASF1 activates shade-responsive gene expression mainly by promoting the H3.3 enrichment. The ASF1-HIRA complex has been reported to promote

FLC gene expression by enhancing H3.3 levels during flowering (Zhao et al., 2021). Incorporation of H3.3 into nucleosome likely modulates higher-order chromatin folding, resulting in an open chromatin conformation (Chen et al., 2013). Nucleosomes are unstable and prone to disassembly, and this instability seems to facilitate the access of transcription factors or other chromatin-associated factors to these regulatory sites (Grover et al., 2018; Jin et al., 2009; Venkatesh and Workman, 2015). ASF1 can promote H3K56ac in heat stress-related genes to induce gene expression under heat stress conditions (Weng et al., 2014). H3.3 deposition has been reported to be correlated with H3K4me3 and H3K36me3 levels, which are associated with gene activation (Daury et al., 2006; Loyola et al., 2006; Zhao et al., 2021). However, significant differences were not detected in either H3K4me3 or H3K36me3 levels in *YUC8*, *PRE1*, and *IAA19* after 1 h of shade treatment (Peng et al., 2018). It will be interesting to further explore the histone modifications that accompany H3.3 under shade conditions.

In addition to the PIF7-ASF1-HIRA regulatory module, which plays pivotal roles in SAS, PIF7, together with its homolog PIF4, are important for thermomorphogenesis (Chung et al., 2020; Fiorucci et al., 2020). Shade avoidance responses share phenotypic patterns similar to that of thermomorphogenesis (Ballare and Pierik, 2017; Burko et al., 2022). Both shade and elevated temperature can deactivate phyB, leading to increased PIFs and elongation (Ballare and Pierik, 2017; Legris et al., 2016). Similar to *pif4* or *pif7-1*, defective hypocotyl elongation was also found in *asf1ab* and *hira-1* at 29 °C, suggesting a role of PIF7-ASF1-HIRA complex in thermomorphogenesis (Appendix Fig S3). However, whether ASF1-HIRA functions together with PIFs in thermomorphogenesis remains to be investigated further.

Based on the results of our study, we propose a working model for how ASF1 activates the transcription on a subset of PIF7 target genes (Fig 6F).

Shade induces the dephosphorylation of PIF7, and enhances PIF7 DNA-binding activity (Li et al., 2012; Willige et al., 2021; Yang et al., 2021). Transcription factor PIF7 mainly binds to promoters and recruits other factors to induce gene expression (Peng et al., 2018; Willige et al., 2021). One of factors recruited by PIF7 is ASF1, which affect H3.3 enrichment with the help of HIRA. Our results demonstrate that PIF7-ASF1-HIRA function on the enrichment of H3.3 and promote gene expression, leading to morphological changes in plants in response to shade.

Materials and Methods

Genetic material and growth conditions. All *Arabidopsis thaliana* plants used in this study were of the Col-0 ecotype. The mutants used in this study have been previously described: *pif7-1*, *phyB-9*, and *PIF7-Flash* (Li et al., 2012); *pifq* (Yang et al., 2021); *asf1a*, *asf1b*, and *asf1ab* (Zhu et al., 2011); *hira-1* (Nie et al., 2014). *HTR5-HA* transgenic plants were obtained by transformation of Col-0, *pif7-1*, *asf1ab*, and *hira-1* with vectors containing the *HTR5* genomic DNA. *HTR13-HA* transgenic plants were obtained by transformation of Col-0 with vectors containing the *HTR13* genomic DNA. Full-length *ASF1A* cDNA was amplified using PCR and ligated into *pCambia1300* to generate *pCambia1300-GFP-ASF1A*. These constructs were transferred into *Agrobacterium tumefaciens* strain *GV3101* (WEIDI, Shanghai, China). Transgenic plants were screened on half-strength Murashige and Skoog (1/2 MS) nutrient medium (Duchefa Biochemie, Haarlem, Netherlands) containing hygromycin and confirmed using immunoblot analysis. We generated *pif7-1 * asf1ab*, *pif7-1 * hira-1*, *phyB-9 * asf1ab*, *phyB-9 * hira-1*, and *GFP-ASF1A * PIF7-Flash* plants via crossing. Double mutants were generated by genetic crossing and were verified using phenotypic inspection, PCR genotyping, and/or sequencing.

For phenotypic analysis, seeds were allowed to germinate on plates containing 1/2 MS medium (Duchefa Biochemie, Haarlem, Netherlands) with 1% agar (Sangon, Shanghai, China) and without sucrose. After stratification, the plates were incubated in growth chambers under continuous white light (R, ~20 μmol m^{-2} s^{-1}; B, ~20 μmol m^{-2} s^{-1}; FR, ~5 μmol m^{-2} s^{-1}) for 4 d at 22℃. The plates were either left in white light or transferred to simulated shade (R, ~20 μmol m^{-2} s^{-1}; B, ~20 μmol m^{-2} s^{-1}; FR, ~60 μmol m^{-2} s^{-1}) for 4 d before measuring the hypocotyl length. To examine hypocotyl elongation at high temperatures, plants were grown at 22 °C under white light (R, ~20 μmol m^{-2} s^{-1}; B, ~20 μmol m^{-2} s^{-1}; FR, ~5 μmol m^{-2} s^{-1}) for 3-4 d, and were further shifted to 29°C or maintained at 22°C for 4 d. *Nicotiana benthamiana* plants were grown at 26 °C under long-day conditions with 16-h light.

Hypocotyl measurement. Quantitative measurements of hypocotyls were performed on scanned images of seedlings using ImageJ software. At least 20 seedlings were used per treatment or genotype. Kinetics of hypocotyl growth was measured by a commercial high-throughput imaging platform, DynaPlant® (Microlens Technology, Beijing, http://www.dynaplant.cn/en). Seedlings for kinetics measurement were sown on 1/2 MS medium containing 2% phytagel (Solarbio, P8170) and grown under continuous white light, and then the plates were transferred to simulated shade. The images of hypocotyl growth were captured by the DynaPlant® platform once every 15 min for each seedling with the physical resolution of 1.2 μm per pixel. The lengths of new hypocotyl growth in the time-series images were quantified by DynaPlant Analysis software which was provided by the manufacturer. The values shown indicate the means with SEMs.

Firefly luciferase complementation imaging assays. The fragments encoding *PIF7* were amplified by PCR and ligated into a *pCAMBIA2300-nLUC* vector to produce *nLUC-PIF7*. The coding regions of *ASF1A* or *ASF1B* were

amplified by PCR and ligated into *pCAMBIA2300-cLUC* to produce *ASF1A-cLUC* or *ASF1B-cLUC*. The resulting constructs were transformed into *Agrobacterium* strain *GV3101*. *Agrobacterium* cells harboring different constructs were then infiltrated into *N. benthamiana* leaves. Three days after infiltration, luciferin (Promega, USA) (2.5 mM, 0.1% Triton X-100) was spread before LUC activity was monitored by a Tanon 5500 chemical luminescence imaging system (Tanon, China).

Protein pull-down assay. For Figure 1B, in the GST pull-down assay, the SUMO-His-PIF7 protein was incubated with pretreated GST-ASF1A or GST-ASF1B beads for 2 h. GST was used as the negative control. The beads were resuspended in SDS-PAGE loading buffer and analyzed by SDS-PAGE and immunoblotting using the anti-His antibody (GNI4110-HS).

For Appendix Figure S2B, in a semi-*in vivo* pull-down assay, total protein was extracted from *GFP-ASF1A* plants grown in duplicate under white light for 8 d using extraction buffer (100 mM Tris-HCl [pH 7.5], 300 mM NaCl, 2 mM EDTA, 1% Trion X-100, 10% glycerol, and protease inhibitor cocktail). Protein extracts were centrifuged at 20,000 × g for 10 min, and the resulting supernatant was incubated with pretreated TF-His-PIF7 beads for 2 h. GFP was used as the negative control. Beads were resuspended in SDS-PAGE loading buffer, analyzed using SDS-PAGE, and followed by immunoblotting using the anti-GFP antibody (GNI4110-GP). For Figure 1C, total protein was extracted from *PIF7-Flash* plants grown in duplicate under white light for 8 d, thereafter, one of the duplicates was treated with shade for 1 h, and the other was maintained under white light for an additional 1 h. Protein extracts were centrifuged at 20,000 × g for 10 min, and the resulting supernatant was incubated with pretreated GST-ASF1A or GST-ASF1B beads for 2 h. GST was used as the negative control. The beads were resuspended in SDS-PAGE loading buffer and analyzed by SDS-PAGE and immunoblotting using the anti-MYC antibody (GNI4110-MC).

Co-IP assay. Total protein extracts were prepared from *GFP-ASF1A * PIF7-Flash* seedlings grown in duplicate under white light for 8 d; thereafter, one of the duplicates was treated with shade for 1 h, and the other was maintained under white light for an additional hour. A Co-IP assay was performed as previously (Peng et al., 2018). IP was performed using anti-MYC agarose beads. Input and IP-resulting fractions were analyzed by western blotting using anti-MYC and anti-GFP antibodies.

RNA-Seq Analysis. RNA-seq was performed as previously described (Yang et al., 2020). In brief, seedlings were grown under white light conditions for 6 d and treated with 1 h shade. Three biological replicates were prepared for each genotype of the plants grown under light and shade conditions. Total RNA was extracted from snap-frozen tissues using TRIzol reagent according to the manufacturer's instructions (Invitrogen). RNA libraries were constructed and sequenced using Majorbio (http://www.majorbio.com/). Differential expression analysis was performed using DESeq2 with |log2foldchange| > log2(2) and *P*-value < 0.01.

Quantitative RT-PCR analysis. Approximately 100 mg of seedlings grown on 1/2 MS media supplemented with 1% agar under different light conditions were collected in Eppendorf tubes, frozen in liquid nitrogen, and ground to a fine powder. Three biological replicates were prepared for each genotype of the plants grown under light and shade conditions. Total RNA was extracted using a TRIzol kit (Promega, USA). Two micrograms of total RNA were reverse transcripted using a First Strand cDNA Synthesis Kit (TIANGEN, China) according to the manufacturer's instructions. The cDNAs were then subjected to real-time qPCR using a CFX Connect Real-Time System (Bio-Rad, USA) and SYBR Green qPCR Mix (Mei5 Biochem, China). Three biological replicates per sample were used for the qRT-PCR analysis. The data are presented as means with the SDs of three biological replicates normalized to the expression of the reference gene *AT2G39960* (Li et al., 2012). The

comparative ΔΔCt method was used to evaluate the relative quantities of each amplified product in the samples. The specificity of the qRT-PCR reactions was determined by melt curve analysis of the amplified products using the standard method. Primers used are listed in Table EV5.

ChIP-Seq Analysis. ChIP-seq assays were performed as previously described (Yang et al., 2020). For *GFP-ASF1A*, *HTR13-HA*/Col-0, *HTR5-HA*/Col-0, and *HTR5-HA/pif7-1* ChIP-seq, two biological replicates were prepared for each genotype of plants grown under light and shade conditions. White light grown seedlings treated with 1 h shade was quickly plucked from plates to perform ChIP assays. Approximately 4 g fresh seedlings were collected and treated with Fix Buffer [0.4 M sucrose, 10 mM Tris-HCl (pH 8.0), 1 mM EDTA, 1 mM PMSF, 1% formaldehyde, 1 × protease inhibitor cocktail tablet (Roche)] under vacuum for about 15 min. Fixation was quenched by adding 0.125 M glycine and infiltrated for 7 min, after which the seedlings were washed three times with cold water and rapidly frozen with liquid nitrogen. The tissue was resuspended in extraction buffer 1 [0.4 M sucrose, 10 mM Tris-HCl (pH 8.0), 10 mM MgCl2, 5 mM β-ME, 0.1 mM PMSF, 1 x protease inhibitor cocktail tablet] and mixed at 4°C for 20 min. The lysate was filtered through Miracloth and centrifuged at 4,000 rpm for 20 min at 4°C. The precipitate was resuspended in extraction buffer 2 [0.25 M Sucrose, 1% Triton X-100, 10 mM Tris-HCl (pH 8.0), 10 mM MgCl2, 5 mM β-ME, 0.1 mM PMSF, 1 x protease inhibitor cocktail tablet] and centrifuged at 12,000 × g for 10 min at 4 °C. The pellet was then resuspended in 300 μL extraction buffer 3 [1.7 M sucrose, 0.15% Triton X-100, 10 mM Tris-HCl (pH 8.0), 10 mM MgCl2, 5 mM β-ME, 0.1 mM PMSF, 1 x protease inhibitor cocktail tablet]. Extraction buffer 3 (450 μL) was layered and centrifuged at 16,000 x g for 1 h at 4 °C. Nuclei were sonicated in 300 μL Nuclei lysis buffer [1% SDS, 50 mM Tris-HCl (pH 8.0), 10 mM EDTA, 1 × protease inhibitor cocktail tablet], and DNA was sheared on a Bioruptor Next Gen UCD-300 (Diagenode Co., Ltd., Toyama, Japan) for 15 cycles of 30/30 s

on/off. The mixture was then centrifuged at 13,200 rpm for 10 min at 4 °C. Four times volume of ChIP Dilution Buffer [1.1% Triton X-100, 1.2 mM EDTA, 167 mM Tris-HCL (pH8.0), 167 mM NaCl, 1 x protease inhibitor cocktail tablet] was added to the supernatant. The mixture was incubated overnight at 4 °C with GFP antibody (ab290, Fig 4) and HA antibody (ab9110, Fig 5 and 6). Fifty microliters of Protein A (Life Technologies) were washed with the ChIP dilution buffer three times, and incubated for an additional 1 h. The mixture was then centrifuged at 1,000 rpm for 2 min at 4°C. The beads were washed with 1 mL of the following buffers for 5 min while rotating at 4 °C: 1 x low salt buffer [150 mM NaCl, 0.1% SDS, 1% Triton X-100, 2 mM EDTA, 20 mM Tris-HCl (pH 8)], 1 x high-salt buffer [500 mM NaCl, 0.1% SDS, 1% Triton X-100, 2 mM EDTA, 20 mM Tris-HCl (pH 8.0)], 1 x LiCl wash buffer [250 mM LiCl, 1% NP-40, 1% sodium deoxycholate, 1 mM EDTA, 10 mM Tris-HCl (pH 8.0)], and 2 x TE buffer [10 mM Tris-HCl (pH 8.0), 1 mM EDTA]. The immunocomplex was eluted from the beads twice with elution buffer (1% SDS, 0.1 M NaHCO3) and incubated for 20 min with shaking at 65°C. A total of 20 µL of 5 M NaCl was added, and crosslinking was reversed by incubation at 65°C overnight. Ten microliters of 0.5 M EDTA, 20 µL 1 M Tris-HCl (pH 6.5–8.0), 2 µL 20 mg/mL Proteinase K (Invitrogen), and 3 µL 10 mg/mL RNase A1 was added and the mixture was incubated at 45°C for 1h. DNA was purified using the HiPure Gel Pure DNA Mini Kit (Magen, D2111-02). Purified ChIP DNA was used to prepare Illumina multiplexed sequencing libraries. Libraries were prepared using the Illumina E7630S NEB/NEBNext® Library Quant Kit (Illumina). Amplified libraries were size-selected using 2% gel to capture fragments between 100 and 400 bp. The libraries were quantified using an Agilent 2100 Bioanalyzer (Agilent Technologies). Samples without antibodies were used as input controls.

The sample library was sequenced on a NovaSeq6000 PE150 by Shanghai Jiayin Biotechnology Ltd. (http://www.rainbow-genome.com/). A

quality distribution plot and base content distribution were generated using FASTQC. Before read mapping, clean reads were obtained from the raw reads by removing adaptor sequences. The clean reads were aligned to the reference genome sequences using the BWA program. The bam file was generated using the unique mapped reads as an input file and, using macs2 software for callpeak with cutoff fold change > 1.5 and *P*-value < 0.01. The input file was the peak file and genome fasta file. The DNA sequence was extracted according to the peak file, and the sequence was compared with the motif database to obtain the motif. Read distributions (bigwig file of IP to subtract input) across genes are presented as an average plot. For statistical difference peak analysis, we merged the peak files of each sample using the bedtools software. The counts of the reads over the bed were determined for each sample using bedtools multicov. Differential accessible peak was assessed using DESeq2. Regions were called differentially accessible with cutoff fold change > 1.5 and *P*-value < 0.01. DAVID was used to identify gene ontology enrichment in the ChIP–seq data.

ChIP-PCR assay. ChIP was performed as previously described (Yang et al., 2020). For @ASF1 (Weng et al., 2014) ChIP, Col-0, *pif7-1*, and *pifq* seedlings were grown under white light for 8 d and then treated with shade for 1 h. Two biological replicates were prepared (Fig 4G and Appendix Fig S5D). For @HA (ab9110) ChIP, *HTR5-HA*/Col-0, *HTR5-HA/pif7-1*, *HTR5-HA/asf1ab* and *HTR5-HA/hira-1* seedlings were grown under white light for 8 d and then treated with shade for 1 h. The seedlings were harvested and cross-linked for 15 min under vacuum in a cross-linking buffer (extraction buffer 1 with 1% formaldehyde). Cross-linking was terminated with 125 mM glycine (pH 8.0) under vacuum for 5 min, and the seedlings were washed three times in double-distilled water and rapidly frozen. The bioruptor was used at high power with 30 s on/30 s off cycles 15 times until the average chromatin size was approximately 300 bp. An anti-HA affinity gel was used for IP. qRT- PCR was

performed using a kit from Takara to determine the enrichment of immunoprecipitated DNA in the ChIP experiments.

Data availability. All mutants and transgenic lines can be requested from the corresponding authors. RNA-seq and ChIP-seq data have been deposited in the NCBI GEO database with accession number GSE189669 (https://www.ncbi.nlm.nih.gov/geo/query/acc.cgi?acc=GSE189669) and GSE193955 (https://www.ncbi.nlm.nih.gov/geo/query/acc.cgi?acc=GSE193955), respectively.

Acknowledgements

We thank Prof. Aiwu Dong (Fudan University, shanghai, China) for a critical reading of the manuscript. We thank Dr. Danhua Jiang (University of Chinese Academy of Sciences, Beijing, China) for providing the *h3.3kd* mutant seeds. This research was supported by the National Natural Science Foundation of China to L.L. (NSFC32030018, 2017YFA0503800), and C.Y (NSFC32100230), and W.-H.S. received support from the Centre National de la Recherche Scientifique (Laboratoire Interna-tional Associé Plant Epigenetic Research) and the Agence National de la Recherche (ANR-19-CE20-0018).

Disclosure and competing interests statement

The authors declare that they have no conflict of interest.

References

Ahmad, K., and Henikoff, S. (2002). The histone variant H3.3 marks active chromatin by replication-independent nucleosome assembly. Mol Cell *9*, 1191-1200.

Ballare, C.L., and Pierik, R. (2017). The shade-avoidance syndrome: multiple signals and ecological consequences. Plant Cell Environ *40*, 2530-2543.

Burko, Y., Willige, B.C., Seluzicki, A., Novak, O., Ljung, K., and Chory, J. (2022). PIF7 is a master regulator of thermomorphogenesis in shade. Nat Commun *13*, 4942.

Casal, J.J. (2013). Photoreceptor signaling networks in plant responses to shade. Annu Rev Plant Biol *64*, 403-427.

Chen, P., Zhao, J., Wang, Y., Wang, M., Long, H., Liang, D., Huang, L., Wen, Z., Li, W., Li, X*., et al.* (2013). H3.3 actively marks enhancers and primes gene transcription via opening higher-ordered chromatin. Genes Dev *27*, 2109-2124.

Chung, B.Y.W., Balcerowicz, M., Di Antonio, M., Jaeger, K.E., Geng, F., Franaszek, K., Marriott, P., Brierley, I., Firth, A.E., and Wigge, P.A. (2020). An RNA thermoswitch regulates daytime growth in Arabidopsis. Nat Plants *6*, 522-532.

Daury, L., Chailleux, C., Bonvallet, J., and Trouche, D. (2006). Histone H3.3 deposition at E2F-regulated genes is linked to transcription. Embo Rep *7*, 66-71.

Duc, C., Benoit, M., Detourne, G., Simon, L., Poulet, A., Jung, M., Veluchamy, A., Latrasse, D., Le Goff, S., Cotterell, S*., et al.* (2017). Arabidopsis ATRX Modulates H3.3 Occupancy and Fine-Tunes Gene Expression. Plant Cell *29*, 1773-1793.

Eitoku, M., Sato, L., Senda, T., and Horikoshi, M. (2008). Histone chaperones: 30 years from isolation to elucidation of the mechanisms of nucleosome assembly and disassembly. Cell Mol Life Sci *65*, 414-444.

English, C.M., Adkins, M.W., Carson, J.J., Churchill, M.E., and Tyler, J.K. (2006). Structural basis for the histone chaperone activity of Asf1. Cell *127*, 495-508.

Fernandez-Milmanda, G.L., and Ballare, C.L. (2021). Shade Avoidance: Expanding the Color and Hormone Palette. Trends Plant Sci *26*, 509-523.

Fiorucci, A.S., Galvão, V.C., Ince, Y., Boccaccini, A., Goyal, A., Allenbach Petrolati, L., Trevisan, M., and Fankhauser, C. (2020). PHYTOCHROME INTERACTING FACTOR 7 is important for early responses to elevated temperature in Arabidopsis seedlings. New Phytol *226*, 50-58.

Galvao, V.C., Fiorucci, A.S., Trevisan, M., Franco-Zorilla, J.M., Goyal, A., Schmid-Siegert, E., Solano, R., and Fankhauser, C. (2019). PIF transcription factors link a neighbor threat cue to accelerated reproduction in Arabidopsis. Nat Commun *10*, 4005.

Grover, P., Asa, J.S., and Campos, E.I. (2018). H3-H4 Histone Chaperone Pathways. Annu Rev Genet *52*, 109-130.

Horard, B., Sapey-Triomphe, L., Bonnefoy, E., and Loppin, B. (2018). ASF1 is required to load histones on the HIRA complex in preparation of paternal chromatin assembly at fertilization. Epigenet Chromatin *11*, 19.

Huang, X., Zhang, Q., Jiang, Y., Yang, C., Wang, Q., and Li, L. (2018). Shade-induced nuclear localization of PIF7 is regulated by phosphorylation and 14-3-3 proteins in Arabidopsis. eLife *7*, e31636.

Jiang, Y., Yang, C., Huang, S., Xie, F., Xu, Y., Liu, C., and Li, L. (2019). The ELF3-PIF7 Interaction Mediates the Circadian Gating of the Shade Response in Arabidopsis. iScience *22*, 288-298.

Jin, C.Y., Zang, C.Z., Wei, G., Cui, K.R., Peng, W.Q., Zhao, K.J., and Felsenfeld, G. (2009). H3.3/H2A.Z double variant-containing nucleosomes mark 'nucleosome-free regions' of active promoters and other

regulatory regions. Nat Genet *41*, 941-5.
Kadauke, S., and Blobel, G.A. (2009). Chromatin loops in gene regulation. Biochim Biophys Acta *1789*, 17-25.
Kim, J., Bordiya, Y., Kathare, P.K., Zhao, B., Zong, W., Huq, E., and Sung, S.B. (2021). Phytochrome B triggers light-dependent chromatin remodelling through the PRC2-associated PHD finger protein VIL1. Nat Plants *7*, 1213-1219.
Legris, M., Klose, C., Burgie, E.S., Rojas, C.C., Neme, M., Hiltbrunner, A., Wigge, P.A., Schafer, E., Vierstra, R.D., and Casal, J.J. (2016). Phytochrome B integrates light and temperature signals in Arabidopsis. Science *354*, 897-900.
Leivar, P., and Quail, P.H. (2011). PIFs: pivotal components in a cellular signaling hub. Trends Plant Sci *16*, 19-28.
Li, L., Ljung, K., Breton, G., Schmitz, R.J., Pruneda-Paz, J., Cowing-Zitron, C., Cole, B.J., Ivans, L.J., Pedmale, U.V., Jung, H.S*., et al.* (2012). Linking photoreceptor excitation to changes in plant architecture. Genes Dev *26*, 785-790.
Loyola, A., Bonaldi, T., Roche, D., Imhof, A., and Almouzni, G. (2006). PTMs on H3 variants before chromatin assembly potentiate their final epigenetic state. Mol Cell *24*, 309-316.
McKittrick, E., Gaften, P.R., Ahmad, K., and Henikoff, S. (2004). Histone H3.3 is enriched in covalent modifications associated with active chromatin. P Natl Acad Sci USA *101*, 1525-1530.
Moshkin, Y.M., Armstrong, J.A., Maeda, R.K., Tamkun, J.W., Verrijzer, P., Kennison, J.A., and Karch, F. (2002). Histone chaperone ASF1 cooperates with the Brahma chromatin-remodelling machinery. Genes Dev *16*, 2621-2626.
Natsume, R., Eitoku, M., Akai, Y., Sano, N., Horikoshi, M., and Senda, T. (2007). Structure and function of the histone chaperone CIA/ASF1 complexed with histones H3 and H4. Nature *446*, 338-341.
Nie, X., Wang, H.F., Li, J., Holec, S., and Berger, F. (2014). The HIRA complex that deposits the histone H3.3 is conserved in Arabidopsis and facilitates transcriptional dynamics. Biol Open *3*, 794-802.
Otero, S., Desvoyes, B., and Gutierrez, C. (2014). Histone H3 dynamics in plant cell cycle and development. Cytogenet Genome Res *143*, 114-124.
Paik, I., Kathare, P.K., Kim, J.I., and Huq, E. (2017). Expanding Roles of PIFs in Signal Integration from Multiple Processes. Mol Plant *10*, 1035-1046.
Peng, M.L., Li, Z.P., Zhou, N., Ma, M.M., Jiang, Y.P., Dong, A.W., Shen, W.H., and Li, L. (2018). Linking PHYTOCHROME-INTERACTING FACTOR to Histone Modification in Plant Shade Avoidance. Plant Physiol *176*, 1341-1351.
Prado, F., Cortes-Ledesma, F., and Aguilera, A. (2004). The absence of the yeast chromatin assembly factor Asf1 increases genomic instability and sister chromatid exchange. Embo Rep *5*, 497-502.
Ramey, C.J., Howar, S., Adkins, M., Linger, J., Spicer, J., and Tyler, J.K. (2004). Activation of the DNA damage checkpoint in yeast lacking the histone chaperone anti-silencing function 1. Mol Cell Biol *24*, 10313-10327.
Reed, J.W., Nagpal, P., Poole, D.S., Furuya, M., and Chory, J. (1993). Mutations in the gene for the red/far-red light receptor phytochrome B alter cell elongation and physiological responses throughout Arabidopsis development. Plant Cell *5*, 147-157.
Ruberti, I., Sessa, G., Ciolfi, A., Possenti, M., Carabelli, M., and Morelli, G. (2012). Plant adaptation to dynamically changing environment: the shade avoidance response. Biotechnol Adv *30*, 1047-1058.
Schulz, L.L., and Tyler, J.K. (2006). The histone chaperone ASF1 localizes to active DNA replication forks to mediate efficient DNA replication. FASEB J *20*, 488-490.

Shu, H., Nakamura, M., Siretskiy, A., Borghi, L., Moraes, I., Wildhaber, T., Gruissem, W., and Hennig, L. (2014). Arabidopsis replacement histone variant H3.3 occupies promoters of regulated genes. Genome Biol *15*, R62.

Stroud, H., Otero, S., Desvoyes, B., Ramirez-Parra, E., Jacobsen, S.E., and Gutierrez, C. (2012). Genome-wide analysis of histone H3.1 and H3.3 variants in Arabidopsis thaliana. P Natl Acad Sci USA *109*, 5370-5375.

Tagami, H., Ray-Gallet, D., Almouzni, G., and Nakatani, Y. (2004). Histone H3.1 and H3.3 complexes mediate nucleosome assembly pathways dependent or independent of DNA synthesis. Cell *116*, 51-61.

Tang, Y., Poustovoitov, M.V., Zhao, K., Garfinkel, M., Canutescu, A., Dunbrack, R., Adams, P.D., and Marmorstein, R. (2006). Structure of a human ASF1a–HIRA complex and insights into specificity of histone chaperone complex assembly. Nat Struct Mol Biol *13*, 921-929.

Venkatesh, S., and Workman, J.L. (2015). Histone exchange, chromatin structure and the regulation of transcription. Nat Rev Mol Cell Biol *16*, 178-189.

Weng, M.J., Yang, Y., Feng, H.Y., Pan, Z.D., Shen, W.H., Zhu, Y., and Dong, A.W. (2014). Histone chaperone ASF1 is involved in gene transcription activation in response to heat stress in Arabidopsis thaliana. Plant Cell Environ *37*, 2128-2138.

Willige, B.C., Zander, M., Yoo, C.Y., Phan, A., Garza, R.M., Trigg, S.A., He, Y., Nery, J.R., Chen, H., Chen, M.*, et al.* (2021). PHYTOCHROME-INTERACTING FACTORs trigger environmentally responsive chromatin dynamics in plants. Nat Genet *53*, 955-961.

Wollmann, H., Holec, S., Alden, K., Clarke, N.D., Jacques, P.E., and Berger, F. (2012). Dynamic Deposition of Histone Variant H3.3 Accompanies Developmental Remodeling of the Arabidopsis Transcriptome. Plos Genet *8*, e1002658.

Wollmann, H., Stroud, H., Yelagandula, R., Tarutani, Y., Jiang, D., Jing, L., Jamge, B., Takeuchi, H., Holec, S., Nie, X.*, et al.* (2017). The histone H3 variant H3.3 regulates gene body DNA methylation in Arabidopsis thaliana. Genome Biol *18*, 94.

Xiao, J., Jin, R., and Wagner, D. (2017). Developmental transitions: integrating environmental cues with hormonal signaling in the chromatin landscape in plants. Genome Biol *18*, 88.

Yang, C., Huang, S., Zeng, Y., Liu, C., Ma, Q., Pruneda-Paz, J., Kay, S.A., and Li, L. (2021). Two bHLH transcription factors, bHLH48 and bHLH60, associate with phytochrome interacting factor 7 to regulate hypocotyl elongation in Arabidopsis. Cell Rep *35*, 109054.

Yang, C., Yin, L., Xie, F., Ma, M., Huang, S., Zeng, Y., Shen, W.H., Dong, A., and Li, L. (2020). AtINO80 represses photomorphogenesis by modulating nucleosome density and H2A.Z incorporation in light-related genes. P Natl Acad Sci USA *117*, 33679-33688.

Zhang, R., Yang, C., Jiang, Y., and Li, L. (2019). A PIF7-CONSTANS-Centered Molecular Regulatory Network Underlying Shade-Accelerated Flowering. Mol plant *12*, 1587-1597.

Zhao, F.Y., Zhang, H.R., Zhao, T., Li, Z.C., and Jiang, D.H. (2021). The histone variant H3.3 promotes the active chromatin state to repress flowering in Arabidopsis. Plant Physiol *186*, 2051-2063.

Zhao, J., Lu, Z., Wang, L., and Jin, B. (2020). Plant Responses to Heat Stress: Physiology, Transcription, Noncoding RNAs, and Epigenetics. Int J Mol Sci *22*.

Zhou, Y., Park, S.H., Soh, M.Y., and Chua, N.H. (2021). Ubiquitin-specific proteases UBP12 and UBP13 promote shade avoidance response by enhancing PIF7 stability. P Natl Acad Sci USA *118*, e2103633118.

Zhu, Y., Weng, M., Yang, Y., Zhang, C., Li, Z., Shen, W.H., and Dong, A. (2011). Arabidopsis homologues

794 of the histone chaperone ASF1 are crucial for chromatin replication and cell proliferation in plant
795 development. Plant J *66*, 443-455.

796

Figure legends

Figure 1. The histone chaperones ASF1A and ASF1B interact with PIF7

A. Interaction between PIF7 and ASF1A/ASF1B was detected using a luciferase complementation imaging (LCI) assay. N-terminal and C-terminal halves of LUC were fused to ASF1A/ASF1B and PIF7, respectively. Luciferin was infiltrated before the LUC activity was monitored.

B. Interaction between PIF7 and ASF1A/ASF1B was detected using a pull-down assay. SUMO-His-fused PIF7 and GST-ASF1A/ASF1B were purified from *E. coli*.

C. Interaction between PIF7 and ASF1A/ASF1B was detected using a semi-*in vivo* pull-down assay. GST-ASF1A/ASF1B were purified from *E. coli*. PIF7-Flash protein from overexpressing *PIF7-Flash* seedlings grown under white light or 1 h of shade treatment was detected using an anti-MYC antibody.

D. Interaction between PIF7 and ASF1A in *Arabidopsis* was detected using the Co-IP assay. Anti-GFP Sepharose beads were used to precipitate GFP-ASF1A from overexpressing *GFP-ASF1A * PIF7-Flash* seedlings grown under white light or 1 h of shade treatment.

E. Interaction between HIRA and ASF1A was detected using a pull-down assay. TF-His-HIRA and GST-ASF1A were purified from *E. coli*.

F. Interactions between ASF1A and PIF7/HIRA were detected in tobacco leaf cells. The PIF7-Flash, HIRA-HA, and GFP-ASF1A (GFP as control) proteins were co-expressed in tobacco leaf cells. Anti-GFP Sepharose beads were used for Co-IP assay.

Figure 2. The histone chaperones ASF1A and ASF1B positively regulate shade-induced hypocotyl elongation

A. Hypocotyl lengths of Col-0 (wild type), *pif7-1*, *asf1a*, *asf1b*, *asf1ab*, and *hira-1* under white light and shade conditions. Seedlings were grown for 4 d

under continuous white light and either maintained under white light (WL, with white box) or transferred to shade (SH, with grey box) for 4 d. The scale bar represents 2 mm. Different letters indicate significant differences ($P < 0.01$) calculated using one-way ANOVA with Tukey's honest significant difference (HSD) test. At least 20 seedlings were used for each treatment or genotype.

B, C. Growth analysis of Col-0, *pif7-1*, *asf1ab*, and *hira-1* seedlings treated with shade. New hypocotyl growth and real-time growth rates were recorded at 15-min intervals after shade treatment. I to IV representing four phases of growth under shade.

D. Hypocotyl lengths of Col-0, *phyB-9*, *asf1ab*, *phyB-9 * asf1ab*, *hira-1*, and *phyB-9 * hira-1* grown under white light. The scale bar represents 2 mm. Different letters indicate significant differences ($P < 0.01$) calculated using one-way ANOVA with Tukey's HSD test. At least 20 seedlings were used for each treatment or genotype.

E. Hypocotyl lengths of Col-0, *pif7-1*, *asf1ab*, *pif7-1 * asf1ab*, *hira-1*, and *pif7-1 * hira-1* under white light and shade conditions. The scale bar represents 2 mm. Different letters indicate significant differences ($P < 0.01$) calculated using one-way ANOVA with Tukey's HSD test. At least 20 seedlings were used for each treatment or genotype.

Figure 3. The PIF7-ASF1-HIRA regulatory module activates the gene expression under shade

A. Heatmap representing the relative expression levels of shade-induced genes in Col-0, *pif7-1*, *asf1ab*, and *hira-1*. The red and white rows indicate RNA expression at high and low levels, respectively.

B. Boxplot displays the fold changes in shade-induced genes in Col-0, *pif7-1*, *asf1ab*, and *hira-1* by comparing the transcript levels between white light and shade conditions. Different letters indicate significant differences ($P < 0.05$) as determined by one-way ANOVA.

C. Venn diagram shows the 132 PIF7-ASF1-HIRA co-regulated shade-responsive genes.

D. Gene ontology (GO) analysis of 132 PIF7-ASF1-HIRA co-regulated shade-responsive genes. For each point, the size is proportional to the number of genes, and the colors represent the *P*-value.

Figure 4. Shade increases ASF1-enrichment at chromatin of target genes of PIF7

A. Heatmap representing the enriched GFP-ASF1A binding peaks under white light (WL) and shade (SH) conditions. Red and white rows indicate GFP-ASF1A peaks at high and low levels, respectively.

B. Pie chart represents the genomic distribution of shade-induced GFP-ASF1A binding events.

C. Average density plot represents the distribution profile of GFP-ASF1A for shade-induced genes (left) and control genes (right). The *P*-value was calculated in a window from 1kb upstream to TES by Welch's *t*-test.

D. Integrative genomics viewer (IGV) screenshots showing the distribution of GFP-ASF1A enrichment at the *ATHB2*, *PIN7*, *CSLC4*, *BIM1*, *ARL*, and *NPY8 loci*.

E. Average density plot representing the distribution profile of GFP-ASF1A in PIF7-targeted shade-responsive genes. The *P*-value was calculated in a window from 1kb upstream to TES by Welch's *t*-test.

F. Average density plot representing the distribution profile of GFP-ASF1A in GFP-ASF1A bound and PIF7-targeted shade-responsive genes. The *P*-value was calculated in a window from 1kb upstream to TES by Welch's *t*-test.

G. ChIP-PCR analysis of ASF1 enrichment using anti-ASF1A antibodies at the *ATHB2*, *PIN7*, *CSLC4*, *BIM1*, *ARL*, and *NPY8 loci*. Col-0 and *pif7-1* seedlings were grown under continuous white light or transferred to the shade for 1 h.

879 Top panels show a schematic representation of the gene structures. The
880 bottom panels represent the effects of shade on ASF1A enrichment.
881 Shade-increased enrichment of ASF1A was calculated as input% SH minus
882 input% WL. The difference at the P2 locus in Col-0 was normalized to one for
883 each gene. Different letters indicate statistically significant differences (P <
884 0.05) by one-way ANOVA with Tukey's HSD test. The data shown are the
885 mean ± SDs (n = 3, where n refers to technical replicates).

886 **Figure 5. Shade-enriched H3.3 levels at its target genes**

887 A, B. Heatmaps representing genome-wide H3.1 and H3.3 enrichment levels
888 from 2 kb upstream of the TSS to 2 kb downstream of the TES under white
889 light (WL) and shade (SH) conditions. Gradient colors represent enrichment
890 levels. The red and white rows indicate H3.1 / H3.3 enrichment at high and low
891 levels, respectively. TSS: transcription start site; TES: transcription end site.

892 C. Average density plots representing the distribution profiles of H3.3 for
893 shade-induced genes and control genes. The *P*-value was calculated in a
894 window from 1kb upstream to TES by Welch's *t*-test.

895 D. Average density plots representing the distribution profiles of H3.1 for
896 shade-induced genes and control genes. The *P*-value was calculated in a
897 window from TSS to TES by Welch's *t*-test.

898 E. The box-plot represents the expression levels of 1246 protein-coding genes
899 that displayed increased H3.3 levels in response to shade. The paired *t*-test
900 was used for statistical analysis.

901 F. GO analysis of the top 400 genes related to H3.3 enrichment and
902 shade-induced transcription. For each point, the size is proportional to the
903 number of genes, and the colors represent the *P*-value.

904 G. IGV screenshots show the distribution of H3.3 and H3.1 enrichment levels
905 at the *ATHB2*, *PIN7*, *CSLC4*, *BIM1*, *ARL*, and *NPY8 loci*.

H. Hypocotyl lengths of Col-0, *pif7-1*, and *h3.3kd* under white light and shade conditions. The scale bar represents 2 mm. Different letters indicate significant differences ($P < 0.01$) calculated using one-way ANOVA with Tukey's HSD test. At least 20 seedlings were used for each treatment or genotype.

I. Relative expression levels of *ATHB2*, *PIN7*, *CSLC4*, *BIM1*, *ARL*, and *NPY8* in Col-0, *pif7-1*, and *h3.3kd* seedlings grown under white light or shade conditions. The seedlings were grown under white light for 6 d, and then maintained under white light, or transferred to shade for 1 h. Different letters indicate statistically significant differences ($P < 0.05$) by one-way ANOVA with Tukey's HSD test. The data shown are the mean ± SDs (n = 3, n refers to biological replicates).

Figure 6. Shade-enriched H3.3 levels at its target genes probably depend on PIF7-ASF1

A. Heatmap representing genome-wide H3.3 enrichment levels from 2 kb upstream of the TSS to 2 kb downstream of the TES in *pif7-1* under white light (WL) and shade (SH) conditions. Gradient colors represent enrichment levels. The red and white rows indicate H3.3 enrichment at high and low levels, respectively.

B. Heatmap representing shade-increased enrichment of H3.3 at 1246 shade-induced H3.3 genes under Col-0 and *pif7-1* background. Shade-increased enrichment of H3.3 was calculated by enrichment levels of H3.3 under shade minus enrichment levels of H3.3 under white light.

C. Average density plots representing the distribution profile of H3.3 at shade-induced genes (left) and control genes (right) in Col-0 and *pif7-1* background. Enhanced H3.3 levels (enrichment levels of H3.3 under shade minus enrichment levels of H3.3 under white light) are visualized around the TES after shade exposure. The *P*-value was calculated in a window from 1kb upstream to TES by Welch's *t*-test.

D. Average density plots representing the distribution profile of H3.3 at PIF7-targeted shade-responsive genes (left), and GFP-ASF1A bound and PIF7-targeted shade-responsive genes (right) in Col-0 and *pif7-1* background. Enhanced H3.3 levels (enrichment levels of H3.3 under shade minus enrichment levels of H3.3 under white light) are visualized around the TES after shade exposure. The *P*-value was calculated in a window from 1kb upstream to TES by Welch's *t*-test.

E. ChIP-PCR analysis of HTR5 (H3.3) levels at the *ATHB2*, *PIN7*, *CSLC4*, *BIM1*, *ARL*, and *NPY8 loci*. Top panels show a schematic representation of the gene structures. The bottom panels represent the effects of shade on H3.3 enrichment. Shade-increased enrichment of H3.3 was calculated as the input% SH minus input% WL. The difference at the P2 locus in Col-0 was normalized to one for each gene. Different letters indicate statistically significant differences ($P < 0.05$) by one-way ANOVA with Tukey's HSD test. The data shown are the means ± SDs (n = 3, where n refers to biological replicates).

F. Proposed model for shade-induced H3.3 enrichment and active transcription at the targets of PIF7. Under shade conditions, dephosphorylated PIF7 binds to its targets and recruits the ASF1-HIRA complex. Consequently, gene-body-localized H3.3 is enhanced and target genes of PIF7 are activated, leading to hypocotyl elongation.

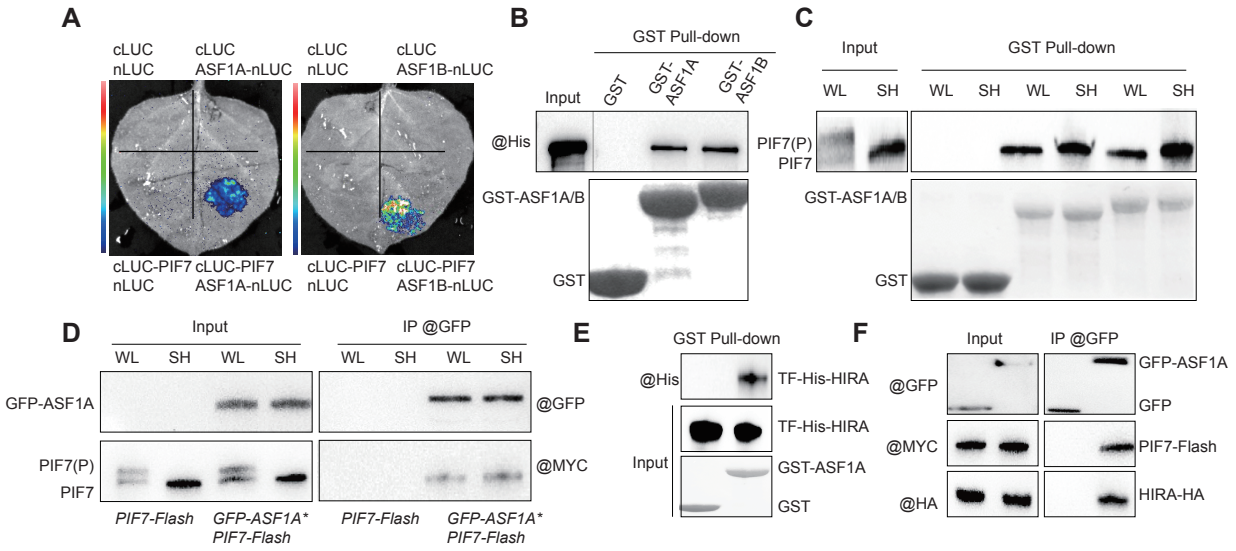

Figure 1. The histone chaperones ASF1A and ASF1B interact with PIF7

A. Interaction between PIF7 and ASF1A/ASF1B was detected using a luciferase complementation imaging (LCI) assay. N-terminal and C-terminal halves of LUC were fused to ASF1A/ASF1B and PIF7, respectively. Luciferin was infiltrated before the LUC activity was monitored.

B. Interaction between PIF7 and ASF1A/ASF1B was detected using a pull-down assay. SUMO-His-fused PIF7 and GST-ASF1A/ASF1B were purified from *E. coli*.

C. Interaction between PIF7 and ASF1A/ASF1B was detected using a semi-*in vivo* pull-down assay. GST-ASF1A/ASF1B were purified from *E. coli*. PIF7-Flash protein from overexpressing *PIF7-Flash* seedlings grown under white light or 1 h of shade treatment was detected using an anti-MYC antibody.

D. Interaction between PIF7 and ASF1A in *Arabidopsis* was detected using the Co-IP assay. Anti-GFP Sepharose beads were used to precipitate GFP-ASF1A from overexpressing *GFP-ASF1A * PIF7-Flash* seedlings grown under white light or 1 h of shade treatment.

E. Interaction between HIRA and ASF1A was detected using a pull-down assay. TF-His-HIRA and GST-ASF1A were purified from *E. coli*.

F. Interactions between ASF1A and PIF7/HIRA were detected in tobacco leaf cells. The PIF7-Flash, HIRA-HA, and GFP-ASF1A (GFP as control) proteins were co-expressed in tobacco leaf cells. Anti-GFP Sepharose beads were used for Co-IP assay.

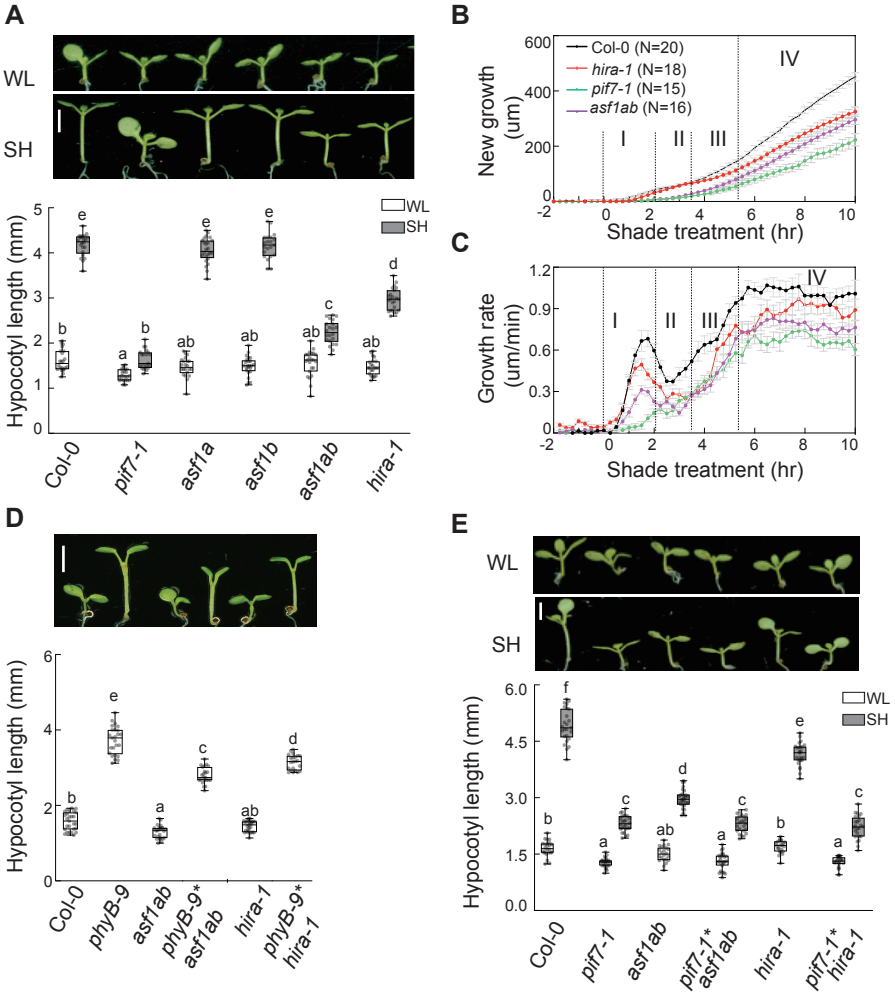

Figure 2. The histone chaperones ASF1A and ASF1B positively regulate shade-induced hypocotyl elongation

A. Hypocotyl lengths of Col-0 (wild type), *pif7-1*, *asf1a*, *asf1b*, *asf1ab*, and *hira-1* under white light and shade conditions. Seedlings were grown for 4 d under continuous white light and either maintained under white light (WL, with white box) or transferred to shade (SH, with grey box) for 4 d. The scale bar represents 2 mm. Different letters indicate significant differences ($P < 0.01$) calculated using one-way ANOVA with Tukey's honest significant difference (HSD) test. At least 20 seedlings were used for each treatment or genotype.

B, C. Growth analysis of Col-0, *pif7-1*, *asf1ab*, and *hira-1* seedlings treated with shade. New hypocotyl growth and real-time growth rates were recorded at 15-min intervals after shade treatment. I to IV representing four phases of growth under shade.

D. Hypocotyl lengths of Col-0, *phyB-9*, *asf1ab*, *phyB-9 * asf1ab*, *hira-1*, and *phyB-9 * hira-1* grown under white light. The scale bar represents 2 mm. Different letters indicate significant differences ($P < 0.01$) calculated using one-way ANOVA with Tukey's HSD test. At least 20 seedlings were used for each treatment or genotype.

E. Hypocotyl lengths of Col-0, *pif7-1*, *asf1ab*, *pif7-1 * asf1ab, hira-1*, and *pif7-1 * hira-1* under white light and shade conditions. The scale bar represents 2 mm. Different letters indicate significant differences ($P < 0.01$) calculated using one-way ANOVA with Tukey's HSD test. At least 20 seedlings were used for each treatment or genotype.

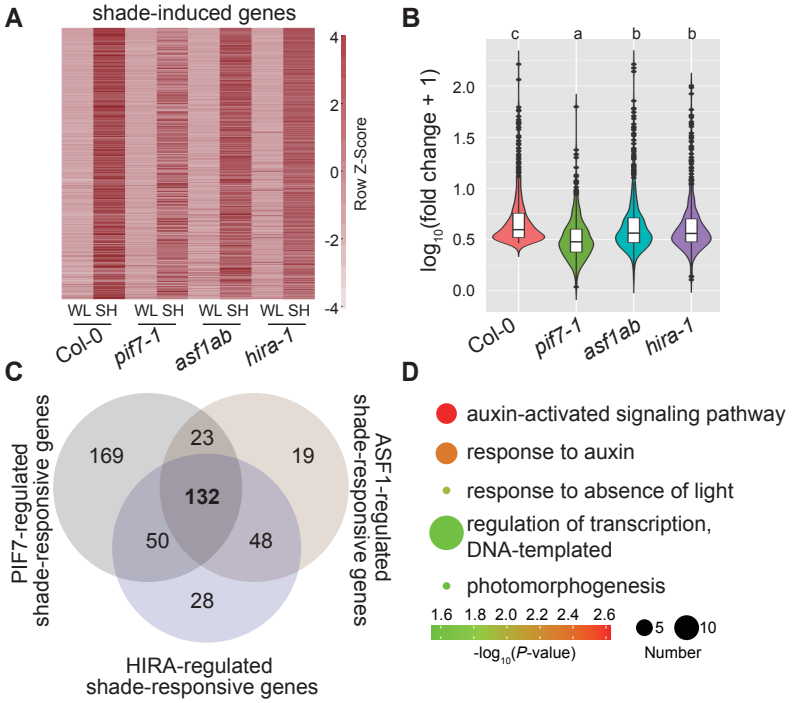

Figure 3. The PIF7-ASF1-HIRA regulatory module activates the gene expression under shade
A. Heatmap representing the relative expression levels of shade-induced genes in Col-0, *pif7-1*, *asf1ab*, and *hira-1*. The red and white rows indicate RNA expression at high and low levels, respectively.
B. Boxplot displays the fold changes in shade-induced genes in Col-0, *pif7-1*, *asf1ab*, and *hira-1* by comparing the transcript levels between white light and shade conditions. Different letters indicate significant differences ($P < 0.05$) as determined by one-way ANOVA.
C. Venn diagram shows the 132 PIF7-ASF1-HIRA co-regulated shade-responsive genes.
D. Gene ontology (GO) analysis of 132 PIF7-ASF1-HIRA co-regulated shade-responsive genes. For each point, the size is proportional to the number of genes, and the colors represent the *P*-value.

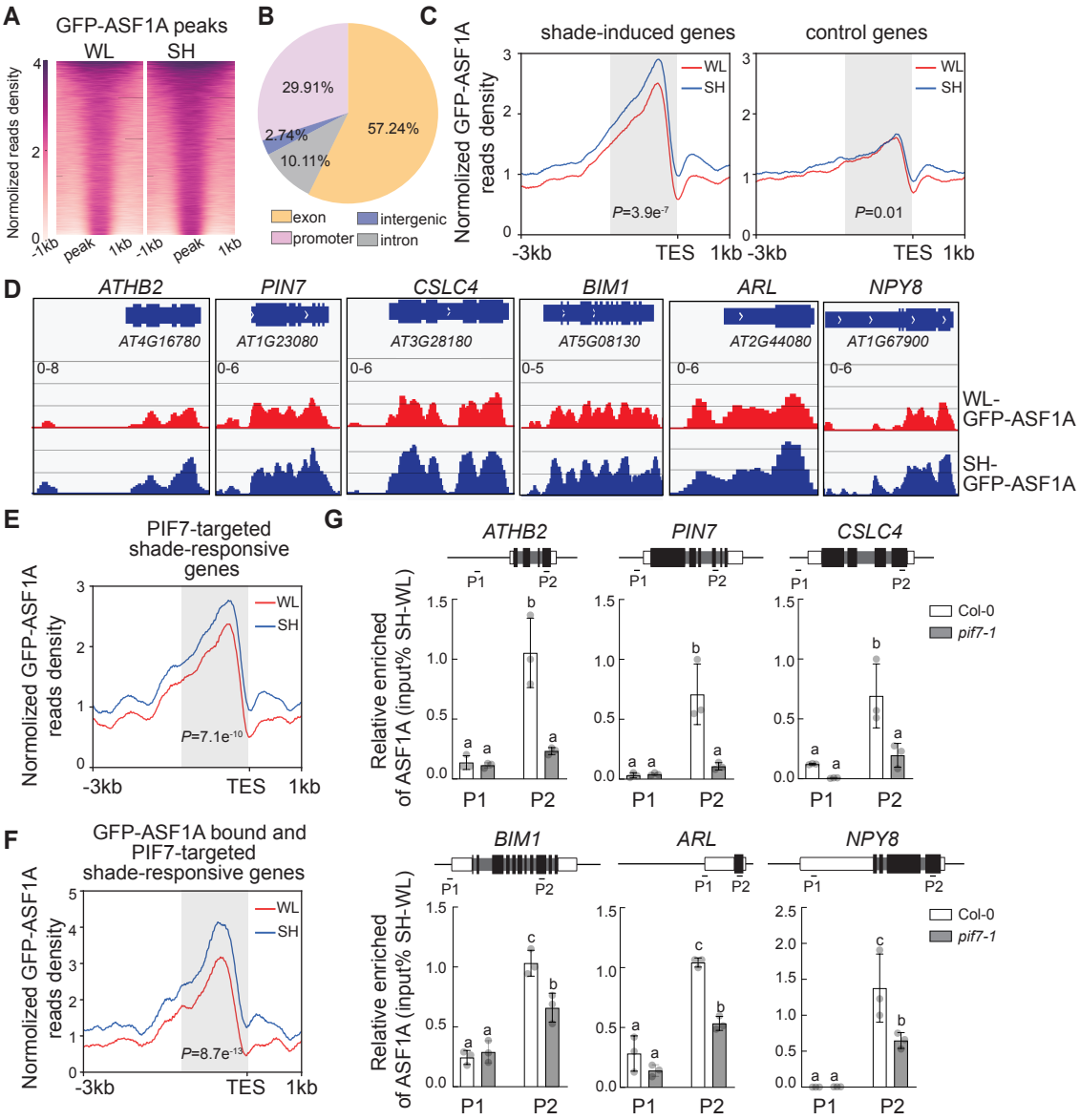

Figure 4. Shade increases ASF1-enrichment at chromatin of target genes of PIF7

A. Heatmap representing the enriched GFP-ASF1A binding peaks under white light (WL) and shade (SH) conditions. Red and white rows indicate GFP-ASF1A peaks at high and low levels, respectively.

B. Pie chart represents the genomic distribution of shade-induced GFP-ASF1A binding events.

C. Average density plot represents the distribution profile of GFP-ASF1A for shade-induced genes (left) and control genes (right). The *P*-value was calculated in a window from 1kb upstream to TES by Welch's *t*-test.

D. Integrative genomics viewer (IGV) screenshots showing the distribution of GFP-ASF1A enrichment at the *ATHB2*, *PIN7*, *CSLC4*, *BIM1, ARL,* and *NPY8 loci*.

E. Average density plot representing the distribution profile of GFP-ASF1A in PIF7-targeted shade-responsive genes. The *P*-value was calculated in a window from 1kb upstream to TES by Welch's *t*-test.

F. Average density plot representing the distribution profile of GFP-ASF1A in GFP-ASF1A bound and PIF7-targeted shade-responsive genes. The *P*-value was calculated in a window from 1kb upstream to TES by Welch's *t*-test.

G. ChIP-PCR analysis of ASF1 enrichment using anti-ASF1A antibodies at the *ATHB2*, *PIN7*, *CSLC4*, *BIM1, ARL,* and *NPY8 loci*. Col-0 and *pif7-1* seedlings were grown under continuous white light or transferred to the shade for 1 h. Top panels show a schematic representation of the gene structures. The bottom panels represent the effects of shade on ASF1A enrichment. Shade-increased enrichment of ASF1A was calculated as input% SH minus input% WL. The difference at the P2 locus in Col-0 was normalized to one for each gene. Different letters indicate statistically significant differences ($P < 0.05$) by one-way ANOVA with Tukey's HSD test. The data shown are the mean ± SDs (n = 3, where n refers to technical replicates).

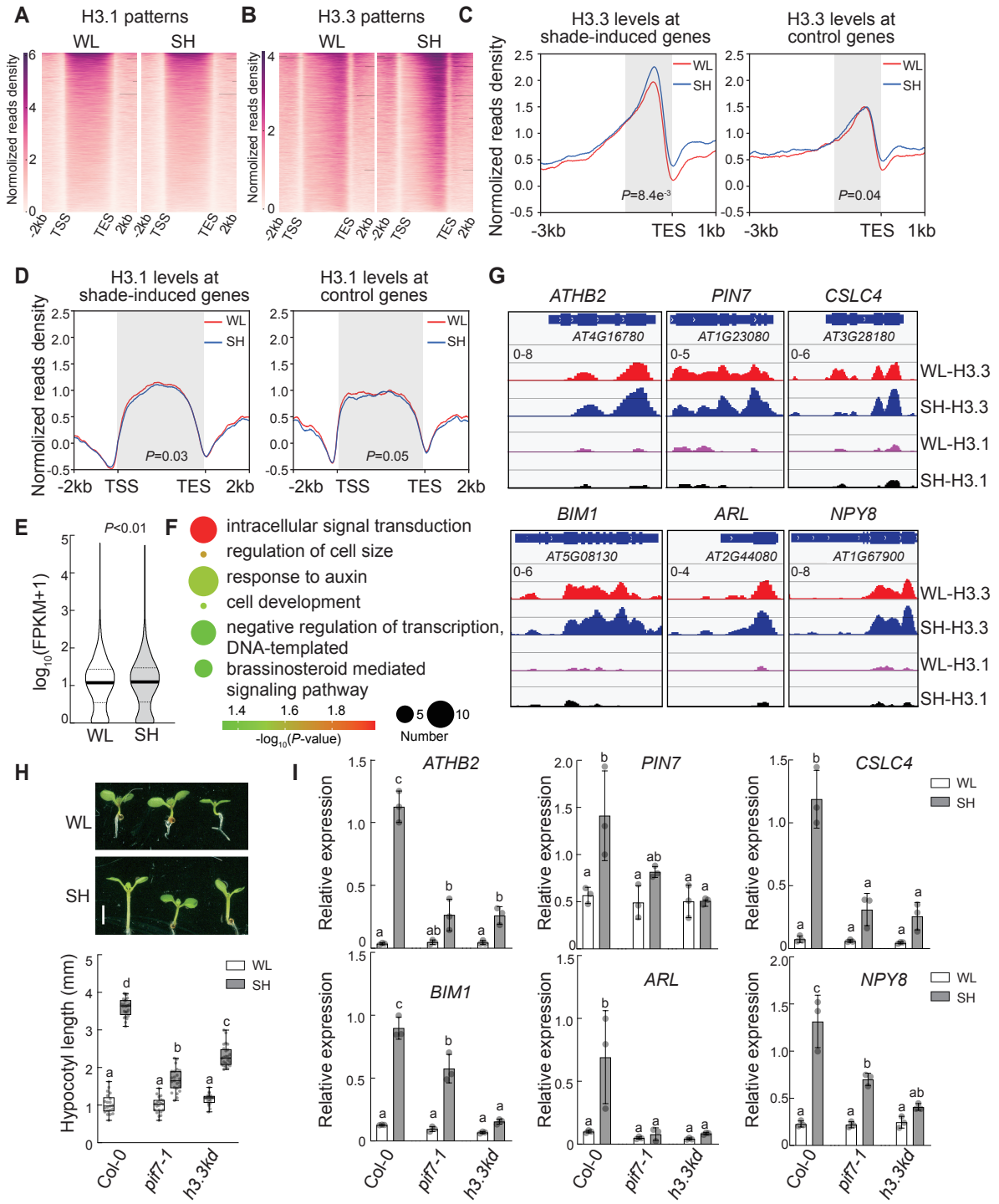

Figure 5. Shade-enriched H3.3 levels at its target genes

A, B. Heatmaps representing genome-wide H3.1 and H3.3 enrichment levels from 2 kb upstream of the TSS to 2 kb downstream of the TES under white light (WL) and shade (SH) conditions. Gradient colors represent enrichment levels. The red and white rows indicate H3.1 / H3.3 enrichment at high and low levels, respectively. TSS: transcription start site; TES: transcription end site.

C. Average density plots representing the distribution profiles of H3.3 for shade-induced genes and control genes. The *P*-value was calculated in a window from 1kb upstream to TES by Welch's *t*-test.

D. Average density plots representing the distribution profiles of H3.1 for shade-induced genes and control genes. The *P*-value was calculated in a window from TSS to TES by Welch's *t*-test.

E. The box-plot represents the expression levels of 1246 protein-coding genes that displayed increased H3.3 levels in response to shade. The paired *t*-test was used for statistical analysis.

F. GO analysis of the top 400 genes related to H3.3 enrichment and shade-induced transcription. For each point, the size is proportional to the number of genes, and the colors represent the *P*-value.

G. IGV screenshots show the distribution of H3.3 and H3.1 enrichment levels at the *ATHB2*, *PIN7*, *CSLC4*, *BIM1, ARL,* and *NPY8 loci*.

H. Hypocotyl lengths of Col-0, *pif7-1*, and *h3.3kd* under white light and shade conditions. The scale bar represents 2 mm. Different letters indicate significant differences ($P < 0.01$) calculated using one-way ANOVA with Tukey's HSD test. At least 20 seedlings were used for each treatment or genotype.

I. Relative expression levels of *ATHB2*, *PIN7*, *CSLC4*, *BIM1, ARL,* and *NPY8* in Col-0, *pif7-1*, and *h3.3kd* seedlings grown under white light or shade conditions. The seedlings were grown under white light for 6 d, and then maintained under white light, or transferred to shade for 1 h. Different letters indicate statistically significant differences ($P < 0.05$) by one-way ANOVA with Tukey's HSD test. The data shown are the mean ± SDs (n = 3, n refers to biological replicates).

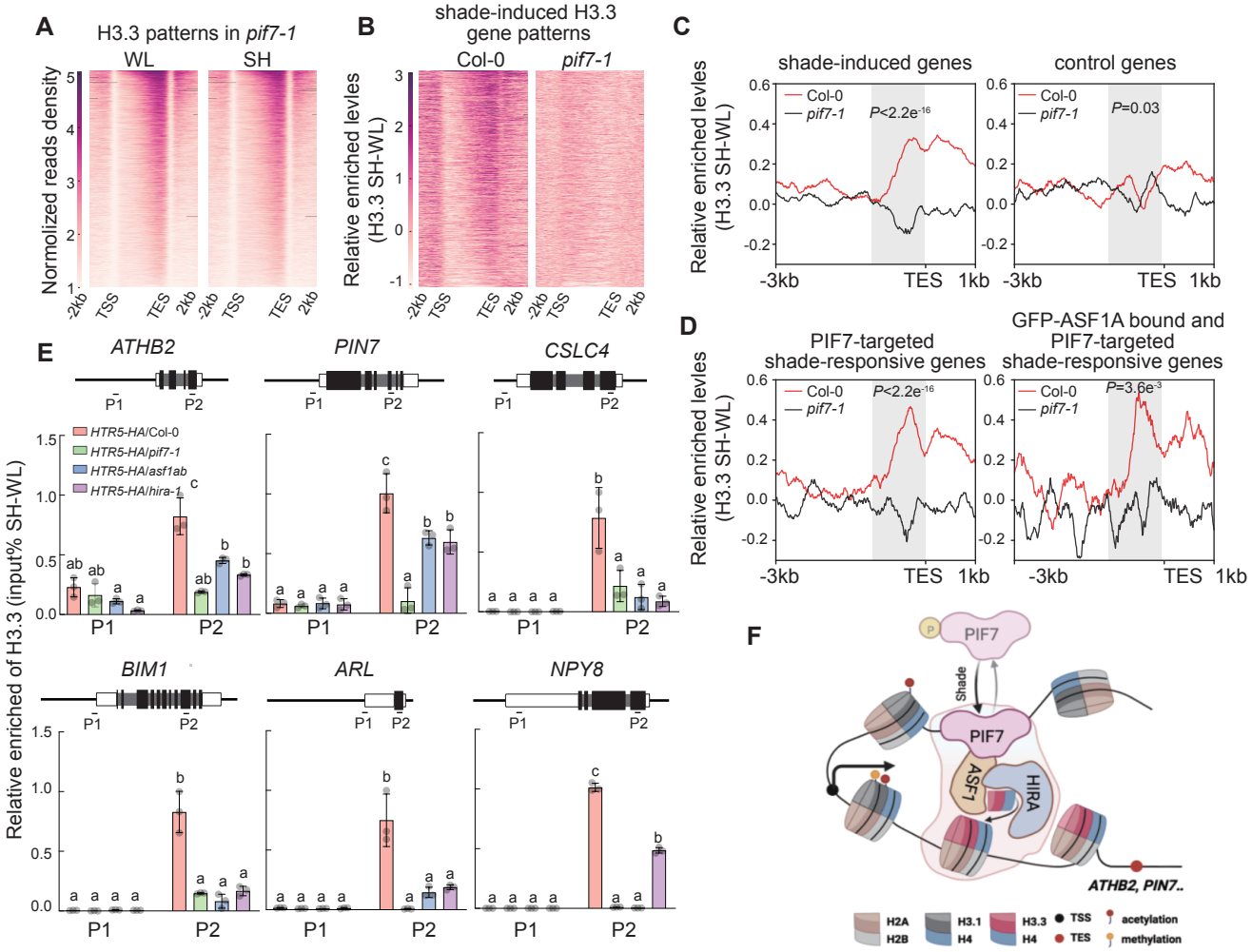

Figure 6. Shade-enriched H3.3 levels at its target genes probably depend on PIF7-ASF1

A. Heatmap representing genome-wide H3.3 enrichment levels from 2 kb upstream of the TSS to 2 kb downstream of the TES in *pif7-1* under white light (WL) and shade (SH) conditions. Gradient colors represent enrichment levels. The red and white rows indicate H3.3 enrichment at high and low levels, respectively.

B. Heatmap representing shade-increased enrichment of H3.3 at 1246 shade-induced H3.3 genes under Col-0 and *pif7-1* background. Shade-increased enrichment of H3.3 was calculated by enrichment levels of H3.3 under shade minus enrichment levels of H3.3 under white light.

C. Average density plots representing the distribution profile of H3.3 at shade-induced genes (left) and control genes (right) in Col-0 and *pif7-1* background. Enhanced H3.3 levels (enrichment levels of H3.3 under shade minus enrichment levels of H3.3 under white light) are visualized around the TES after shade exposure. The *P*-value was calculated in a window from 1kb upstream to TES by Welch's *t*-test.

D. Average density plots representing the distribution profile of H3.3 at PIF7-targeted shade-responsive genes (left), and GFP-ASF1A bound and PIF7-targeted shade-responsive genes (right) in Col-0 and *pif7-1* background. Enhanced H3.3 levels (enrichment levels of H3.3 under shade minus enrichment levels of H3.3 under white light) are visualized around the TES after shade exposure. The *P*-value was calculated in a window from 1kb upstream to TES by Welch's *t*-test.

E. ChIP-PCR analysis of HTR5 (H3.3) levels at the *ATHB2*, *PIN7*, *CSLC4*, *BIM1, ARL,* and *NPY8 loci*. Top panels show a schematic representation of the gene structures. The bottom panels represent the effects of shade on H3.3 enrichment. Shade-increased enrichment of H3.3 was calculated as the input% SH minus input% WL. The difference at the P2 locus in Col-0 was normalized to one for each gene. Different letters indicate statistically significant differences ($P < 0.05$) by one-way ANOVA with Tukey's HSD test. The data shown are the means ± SDs (n = 3, where n refers to biological replicates).

F. Proposed model for shade-induced H3.3 enrichment and active transcription at the targets of PIF7. Under shade conditions, dephosphorylated PIF7 binds to its targets and recruits the ASF1-HIRA complex. Consequently, gene-body-localized H3.3 is enhanced and target genes of PIF7 are activated, leading to hypocotyl elongation.